polymer papers

A generalized Eden model of polymer crystallization

Marc L. Mansfield* and Leonid I. Klushin†
Michigan Molecular Institute, 1910 West St Andrews Road, Midland, MI 48640, USA
(Received 30 August 1993)

A generalization of the Eden model is proposed as a model of polymer crystallization. The model exhibits all three growth regimes. It produces the Seto–Frank model in one limit and demonstrates departures from the Seto–Frank model induced by discreteness of the crystal. It is able to predict curved growth fronts; in fact it predicts that circular crystals are to be expected in regime III.

(Keywords: polymer crystallization; curved edges; generalized Eden model)

INTRODUCTION

Seto[1] in 1964 and Frank[2] in 1974 developed a set of differential equations that describe the growth of polymer crystals. When combined with the kinetic nucleation theory developed by Hoffman and Lauritzen[3–5], the Seto–Frank equations predict a number of properties of polymer crystal growth, including regime transitions and the dependence of macroscopic crystal growth rates on microscopic properties. For some time, therefore, the resulting kinetic nucleation theory has had wide acceptance. This has changed, however, with the observation of single crystals of polymers such as polyethylene and polyoxyethylene that have curved growth fronts[6–12], since the ability of the standard theory to predict the existence of growth fronts with curvature has been brought into question[13–21].

The Seto–Frank equations predict curved growth profiles; under certain conditions, they yield asymptotically exact elliptical growth profiles[22–25]. However, these elliptical growth profiles raise additional questions. For example, to obtain solutions with appreciable curvature requires the suppression, discussed more amply below, of the substrate completion rate, g, by several orders of magnitude[26,27]. Some authors have found this to be objectionable and therefore prefer an interpretation promoted primarily by Sadler[13–21]. He argued that the kinetic process upon which the Lauritzen–Hoffman and Seto–Frank theories are based is fundamentally incorrect, and must be replaced by a thermal roughening transition mechanism. On the other hand, Hoffman and Miller[26,27] have argued that under certain conditions, chain folds are adequate to suppress the substrate completion process and therefore produce curved crystals with morphologies comparable to those observed experimentally.

There is, none the less, an additional problem associated with the elliptical solutions to the Seto–Frank equations: under conditions of appreciable curvature, the Seto–Frank equations are invalid. This is not to say that the elliptical profiles are incorrect solutions to the equations, but rather that the equations themselves have lost validity. The Seto–Frank equations are based on a continuum approximation, and become invalid whenever the granularity of the crystal lattice becomes significant. This limitation also implies that the Seto–Frank equations are unable to predict regime III growth. To understand the limitations of the Seto–Frank equations requires us to study models that retain a discrete crystal lattice, which leads naturally to questions of random growth on lattices.

Models of random lattice growth have attracted considerable attention during the last decade. We will be concerned here with generalization of the so-called Eden growth process[28–52]. The existence of a domain or cluster of lattice cells at time t is assumed. The boundary of the cluster is defined as the set of cells that are not in the cluster but that have at least one nearest neighbour that is. In each time step, one cell is selected at random from the boundary to become a member of the cluster. One is interested in the statistical properties of the cluster as they develop over time. An alternative realization of the Eden model results if, instead of one boundary cell being selected in each step, any given boundary cell joins the cluster with probability p in each step. Obviously the two realizations become equivalent in the limit $p \to 0$, differing only in the flow of time.

In this paper we study a generalization of this second realization. We define four separate probabilities, p_1, p_2, p_3, p_4. If a given boundary cell has j nearest neighbours in the cluster at time t, then that cell joins the cluster with probability p_j during that time step. This model exhibits growth in all three regimes, and allows us to study the development of curved edges etc. In addition, it allows us to examine the limitations to the validity of the Seto–Frank equations.

A number of related growth models have also been considered[53–58]. These generally exhibit all three growth regimes and illuminate many properties of each regime. However, generally they are not concerned with questions of curved edges or of gross crystal morphology.

* To whom correspondence should be addressed
† Present address: Department of Physics, American University of Beirut, Beirut, Lebanon

0032-3861/94/14/2937-07

LIMITATIONS OF THE SETO–FRANK APPROACH

The Seto–Frank equations assume that nuclei appear on a substrate with rate i per unit substrate length and per unit time and that the resulting pair of steps or niches begins to move, one to the left and one to the right, with average velocity $\pm g$, as new crystalline stems add to the two niches[1,2]. These two niches continue to move until they either strike another niche coming from the opposite direction, or until they encounter the boundary of the crystal. There are two relevant quantities derived from i and g, which we will here call the Frank length, L_F, and the Frank velocity, G_F, that are defined as follows:

$$L_F = (2g/i)^{1/2} \quad (1)$$

$$G_F = b(2ig)^{1/2} \quad (2)$$

where b is the lattice spacing. The Frank length is associated with the average distance between niches, while the Frank velocity is simply the regime II growth rate. (Prediction of regime I growth rates in the context of the Seto–Frank equations requires introduction of a third length scale L, representing the overall crystal size. Since such a length is absent in the elliptical-profile treatment, that treatment is inherently regime II.) Since the Seto–Frank treatment neglects the granularity of the lattice, a necessary condition for its validity is $L_F \gg b$. The elliptical-profile solutions state that each growth front of a growing crystal is a section of an ellipse[22–25]. The two axes of the ellipse are in the ratio g/G_F, where g and G_F are the substrate completion rate and overall growth rate as defined for that particular growth front. In the more traditional applications of the theory we have $g \gg G_F$, the ellipses are very elongated, and the associated growth fronts are effectively flat. However, if g decreases relative to G_F, the growth fronts exhibit appreciable curvature.

The condition for appreciable curvature, therefore, is $g \simeq G_F$, which requires, by equations (1) and (2), $L_F \simeq b$, which means that the Seto–Frank treatment is not valid when the growth front is significantly curved. Two other symptoms of the failure of the Seto–Frank equations are, first, that the elliptical-profile solution leads to absurd crystal shapes if $g < G_F$ and second, its inability to predict regime III. In this paper, we consider the properties of a random lattice growth model which exhibits Seto–Frank behaviour in the extreme $g \gg G_F$ but which remains valid as we consider the cases $g \simeq G_F$ and $g < G_F$ since it preserves the discreteness of the lattice.

INTRODUCTION TO THE MODEL

Let us consider a simple square lattice. At any given time, some set of lattice cells are assumed to be painted in, all others not. For example, we will frequently assume that at $t=0$, only the cell at the origin is painted. Then in each discrete time step, each unpainted cell is painted in with one of the four probabilities p_1, p_2, p_3, p_4, if the cell in question has respectively 1, 2, 3 or 4 nearest neighbours that are already painted. In this way, as time advances, the painted region or cluster grows to fill more and more of the lattice, and we are primarily interested in the rate at which the cluster grows and the cluster morphology that eventually develops. This model is a generalization of the Eden model[28–52] which has been proposed as a model for such random growth processes as the spread of epidemics or tumour growth.

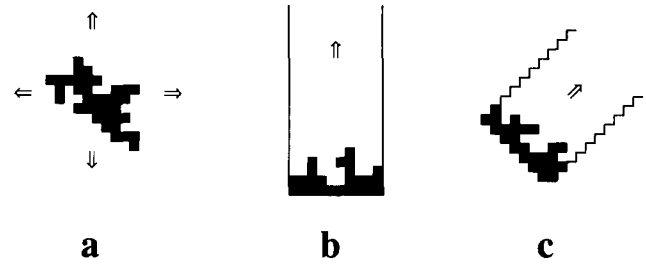

Figure 1 Numerical studies of the model were performed with one of three boundary conditions: (a) open boundaries, growth permitted simultaneously in all directions; (b) and (c) growth down channels, inclined either 0° or 45° relative to the lattice, with periodic boundary conditions

We have primarily employed three different types of boundary conditions, summarized in *Figure 1*. The first type of boundary condition, which we will refer to as the open boundary condition, assumes that only the lattice cell at the origin is painted at $t=0$, and the cluster is permitted to grow simultaneously in all directions. The other two types of boundary conditions consider growth down channels, inclined either at 0° or 45° relative to the lattice direction. These will be called the 0° or 45° channel boundary conditions. These begin at $t=0$ with the lowest tier completely painted in, and then are permitted to develop over time with the assumption of periodic boundary conditions across both walls of the channel.

The probability p_1 corresponds, of course, to the nucleation rate i while the probability p_2 corresponds to the substrate completion rate g. In fact, we form a connection with the kinetic nucleation theory of polymer crystal growth by writing

$$i = \frac{p_1}{b\Delta t} = p_1 \quad (3)$$

$$g = \frac{p_2 b}{\Delta t} = p_2 \quad (4)$$

where b is the lattice spacing and Δt is the duration of the time step in the model. The second equality in each case results from the assumption of length and time units such that $b=1$ and $\Delta t=1$, a convention that will be followed hereafter.

We define two separate growth rates, G_0 and G_{45}, as overall growth rates of the cluster. G_0 represents the rate at which the boundary of the cluster advances in directions parallel to either the x or y axes, since by symmetry these rates must be the same. G_{45} represents the similar quantity defined for directions inclined 45° relative to the x or y axes, i.e. along the diagonals. With the open boundary condition, we estimate G_0 in the $+x$ direction by tracking the progress of the leftmost vertical line lying completely to the right of the cluster, with similar procedures in the $-x$ and the $\pm y$ directions. These four velocities are then averaged. The value of G_0 may be estimated for growth in the 0° channel by keeping track of the rate at which new cells are added. For example, if the channel is L units wide, then the growth front has obviously moved an average of 1 unit every time it adds L cells. The value of G_{45} may be estimated in like manner.

We have found that the cluster grows uniformly in time, whatever the values of p_j. After a relatively short induction period, the cluster assumes a particular shape and a particular radial growth velocity that depend on

the particular values of p_j, and it maintains that same shape and velocity over time.

THE CASE $p_1=p_2=p_3=p_4\equiv p$: THE STANDARD EDEN MODEL

An interesting special case is obtained whenever $p_1=p_2=p_3=p_4\equiv p$. When $p=1$, the growth is completely deterministic, in each time step all nearest neighbours are painted in. After time t the cluster consists of all lattice sites that can be reached in t steps and therefore has the diamond shape shown in *Figure 2*. The two growth rates G_0 and G_{45} are respectively 1 and $2^{-1/2}$. As p decreases, the structure becomes rounded, and approaches the nearly circular habit also shown in *Figure 2*. In the limit $p\to 0$, we recover the standard Eden model[28-52]. The Eden model has been the subject of intense interest recently, with most of the interest centred on the long-time global structure of the cluster, its growth rate, distribution of voids in the cluster, the steady-state structure of the boundary, and the approach to this steady state. The following paragraphs summarize the properties of the Eden model, and of its generalization to non-zero p. These properties are either found in the literature[28-52], or were computed directly by the authors.

The Eden cluster on the simple square lattice has a nearly circular outline that progresses with a constant outward velocity. One surprising aspect is that the outline is not perfectly circular[34,36,38,42,59]. This effect is obvious

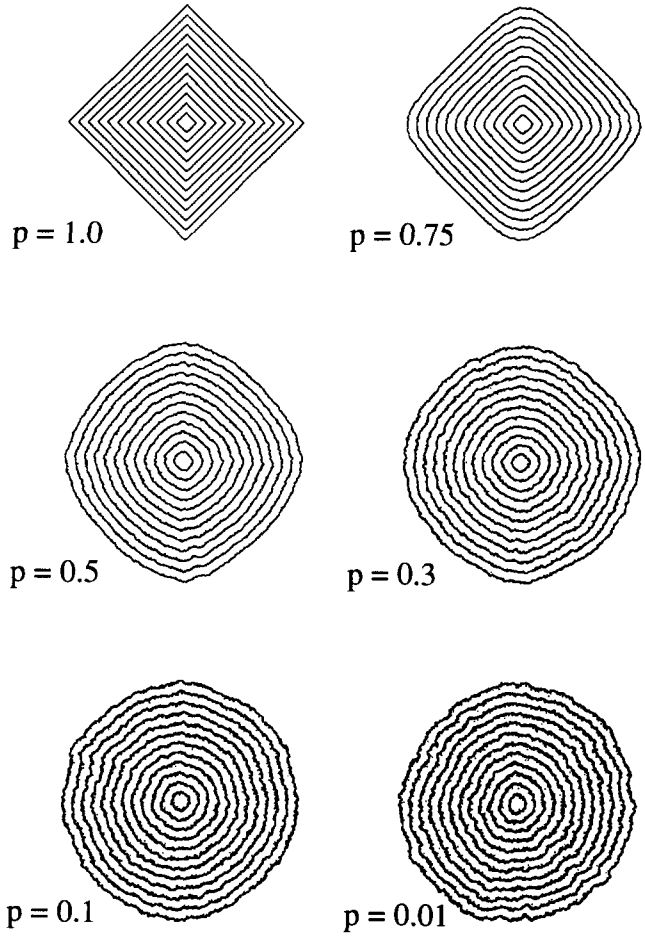

Figure 2 Cluster morphologies obtained when $p_1=p_2=p_3=p_4\equiv p$. For p near 1, lozenge shapes develop; these reflect the discrete time step and are therefore non-physical. For p near 0, the nearly circular clusters of the standard Eden model develop

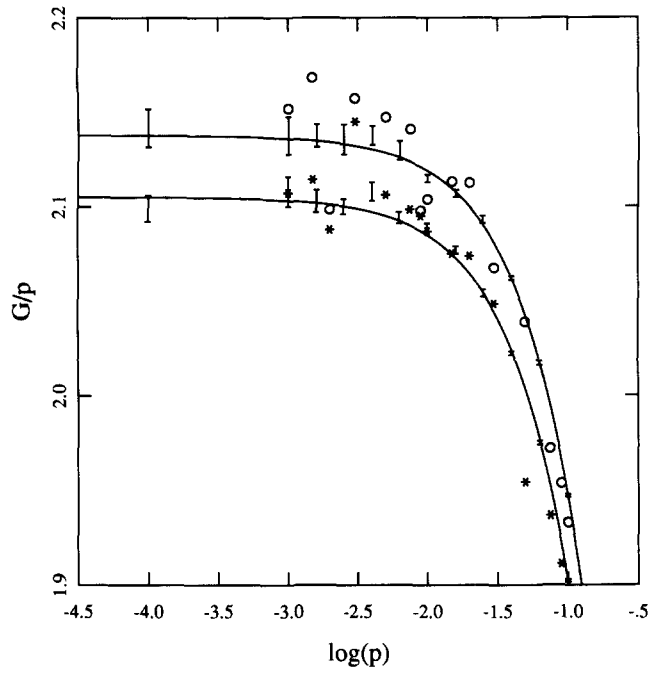

Figure 3 Growth rates obtained when $p_1=p_2=p_3=p_4\equiv p$, displayed here as G_0/p or G_{45}/p. (○) G_0/p computed with open boundaries; (*) G_{45}/p computed with open boundaries; error bars, G_0/p (upper set) or G_{45}/p (lower set) computed with channel boundaries; solid curves, best linear fits, equations (5a) and (5b)

in *Figure 3*, where the two ratios G_0/p and G_{45}/p are plotted as functions of p. These have been computed in a number of different ways. The open circles or asterisks were computed directly from clusters growing with the open boundary conditions shown in *Figure 1a*. The error bars were computed from growth in channels, either at 0° or 45°, and show the value of the mean, plus or minus one standard deviation, obtained from a number of independent runs. (Accuracy in this case is excellent at lower p, where the error bars are very narrow, but deteriorates at small p.) The two sets of data in *Figure 3* are well represented by

$$G_0/p=2.138-1.913p \tag{5a}$$

$$G_{45}/p=2.105-2.037p \tag{5b}$$

which appear in *Figure 3* as solid curves. This slight difference between G_0 and G_{45} obviously implies that the cluster is not completely circular.

We have found that the final steady state values of the growth rates G_0 and G_{45} are obtained only rather slowly, and that the measured values can increase slightly by increasing the duration of the calculation. Therefore, the limiting values of 2.138 and 2.105 reported in equations (5) and (6) are both a few per cent too low. After long, exhaustive runs in channels we conclude that the growth rates obey

$$\lim_{p\to 0}\frac{G_0}{p}=2.167\pm 0.002 \tag{6a}$$

$$\lim_{p\to 0}\frac{G_{45}}{p}=2.127\pm 0.002 \tag{6b}$$

These limiting values are obtained, for growth in channels, only after the growth front has progressed a distance of approximately 200. On the other hand, the overall variations amount to only a few per cent, so we

continue, in what follows, to consider results obtained over shorter runs.

The Eden cluster contains voids: the growth process leaves voids behind as the cluster front moves through a region of space. However, the probability of voids surviving for very long times after the passage of the growth front is very small. Eventually, any given void will be filled and the concentration of voids is only large in the vicinity of the boundary.

The growth rate G_0 computed in the open boundary case is shown as a function of p in *Figure 4*. Obviously, for this model $G_0 = 2.167p$ in the limit $p \to 0$. Near $p = 1$, the curve departs from this proportionality. This is due to the discrete time step; in continuous time we would expect the proportionality to hold universally.

THE CASE $p_1 \ll 1$, $p_2 \ll 1$, $p_3 = p_4 = 1$: A MODEL FOR POLYMER CRYSTAL GROWTH

We now consider the properties of the model in those situations for which the various p_j values are not necessarily equal. Most of our effort has been expended in studying the case where $p_1 \ll 1$, $p_2 \ll 1$, $p_3 = 1$ and $p_4 = 1$. It is important to keep both p_1 and p_2 small to minimize the effects of the discrete time step. On the other hand, we find that the overall growth rate and global morphology of the cluster are insensitive to p_3 and p_4, and therefore typically set p_3 and p_4 to unity. The probabilities p_3 and p_4 influence the way in which the cluster boundary ripens, but have little effect on the way in which the cluster boundary invades new territory.

When grown in the open boundary condition, the model exhibits a regime III→II transition. The value of G_0 in regime II is, according to equations (1)–(4), $(2p_1p_2)^{1/2}$, while in regime III it proves to be given accurately by the standard Eden result of equation (6a), $2.167p_1$. Therefore:

$$G_0 = (2p_1p_2)^{1/2} \quad \text{regime II} \tag{7a}$$

$$G_0 = 2.167p_1 \quad \text{regime III} \tag{7b}$$

with the regime transition occurring where these two velocities cross over one another:

$$p_1/p_2 < 0.426 \quad \rightarrow \text{regime II} \tag{8a}$$

$$p_1/p_2 > 0.426 \quad \rightarrow \text{regime III} \tag{8b}$$

A few results for G_0 obtained with the open boundary condition are shown in *Figure 5*. Note that the actual growth rates are given quite well by equation (7), except when $p_1 \gtrsim 0.1$, when, as already mentioned, the results become sensitive to the discreteness of the time variable.

The gross cluster morphologies prove to be a function only of the ratio p_1/p_2, except when p_1 approaches unity. Several examples are displayed in *Figure 6*. These begin as square crystals with effectively flat edges when $p_1 \ll p_2$. This corresponds to the flat, sectored crystals expected whenever nucleation rates are small. As p_1 approaches p_2 from below, these flat crystals become more and more rounded, in approximate agreement with the predictions of the elliptical-profile treatment. These tend, eventually, to the rounded, nearly circular patterns of the standard Eden mode. In fact, for all values of p_1/p_2 for which we expect regime III by equation (8), we find the overall morphology to be the near circles of the standard Eden model. However, cluster morphology loses dependence on p_1/p_2 when p_1 approaches unity. Then the lozenges first encountered in the last section at large p appear.

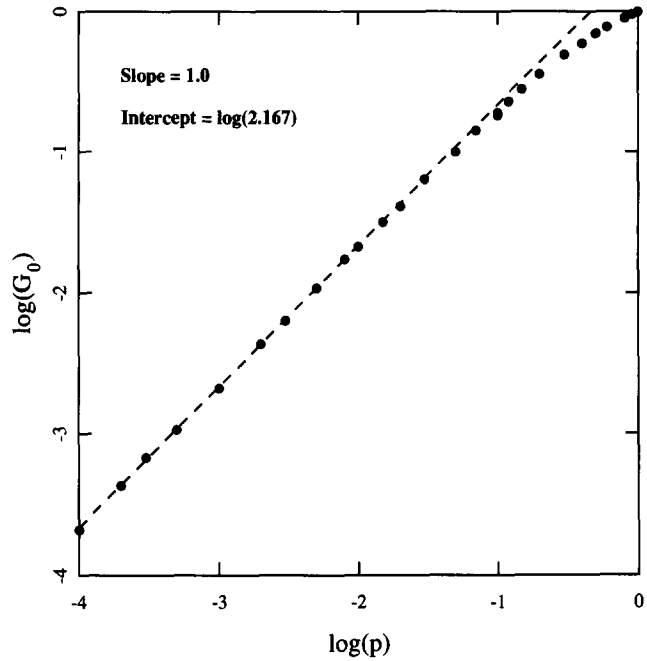

Figure 4 Growth rates G_0 as a function of p for $p_1 = p_2 = p_3 = p_4 \equiv p$

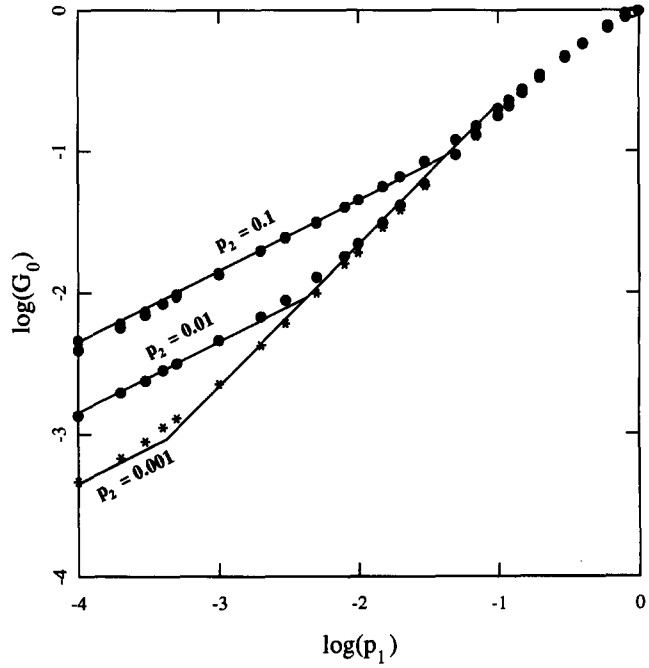

Figure 5 Growth rates G_0 when $p_3 = p_4 = 1$ and when p_1 and p_2 assume the values shown. Solid lines are drawn according to equations (7) and (8)

In order to characterize the structure of the cluster boundary, and to compare these results to those of the elliptical profiles given as solutions to the Seto–Frank equations, we have developed a scheme for fitting an elliptical section to the boundary of the growing cluster. Consistent with the symmetry of the lattice, we employ four equivalent elliptical arcs, as in *Figure 7*, in an attempt to characterize the boundary. Of course, this is not meant to suggest that the clusters have exactly elliptical profiles, but only to obtain the best ellipse that fits the profile. During growth of the profile, in the open

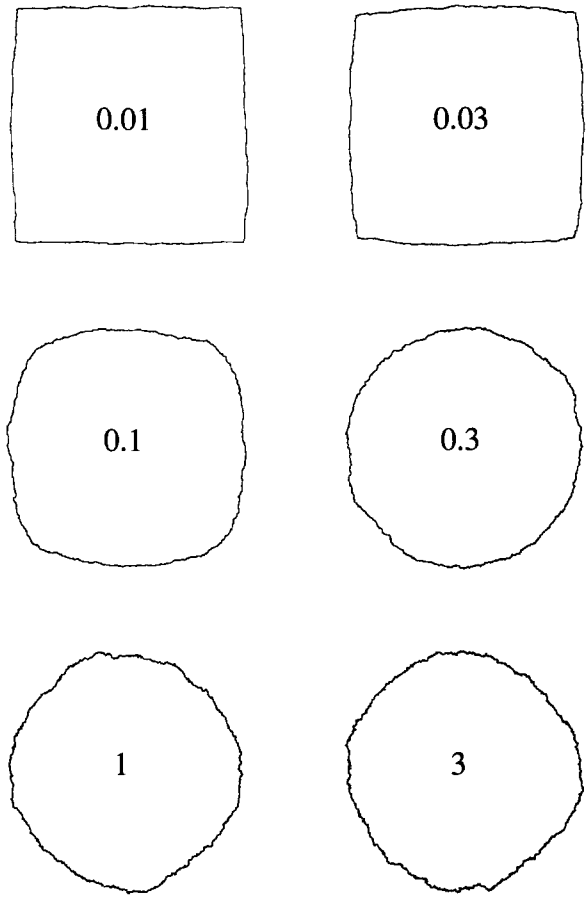

Figure 6 Cluster morphologies obtained when $p_1 \ll 1$, $p_2 \ll 1$ and $p_3 = p_4 = 1$. For these p_j values, the gross morphology is a function of p_1/p_2 only; the p_1/p_2 ratio producing each cluster is shown. As $p_1/p_2 \to 0$, we obtain squares. Whenever $p_1/p_2 \gtrsim 1$ we obtain the near circles of the standard Eden model

boundary condition, the states of the lattice cells (p,q), $(2p,2q)$, $(3p,3q)$, ... are monitored, where p and q are relatively prime integers. The times at which each of these cells join the growing cluster are recorded, from which we are able to estimate a growth rate $G(\theta)$, for θ the polar angle associated with the point (p,q). These are obtained for many different angles θ around the circle, and then averaged over all symmetry-equivalent angles to give a set of $G(\theta)$ data for θ in the interval $45° \leqslant 0 \leqslant 90°$. These polar-coordinate data are converted to a set of Cartesian coordinates x and y, to which this ellipse is fit:

$$\alpha^2 x^2 + y^2 = G_r^2 \tag{9}$$

by standard linear regression, treating x^2 and y^2 as linearly dependent variables. The limit $\alpha \to 0$ corresponds to flat, non-curved edges; when α is near 1 the profile is nearly circular. The quantity G_r in equation (9) corresponds to G_0, at least to the degree that the ellipse of equation (9) corresponds to the actual data. Indeed, the ratio G_r/G_0 measures the goodness of fit.

The Seto–Frank ellipses, as previously mentioned, have axes in the ratio G_0/g, from which it follows that the Seto–Frank prediction for α is simply

$$\alpha = \frac{G_0}{g} = \left(\frac{2p_1}{p_2}\right)^{1/2} \tag{10}$$

This prediction is compared with the results of the present model in *Figure 8*. As stated above, the cluster morphology is seen to be a function of p_1/p_2 only,

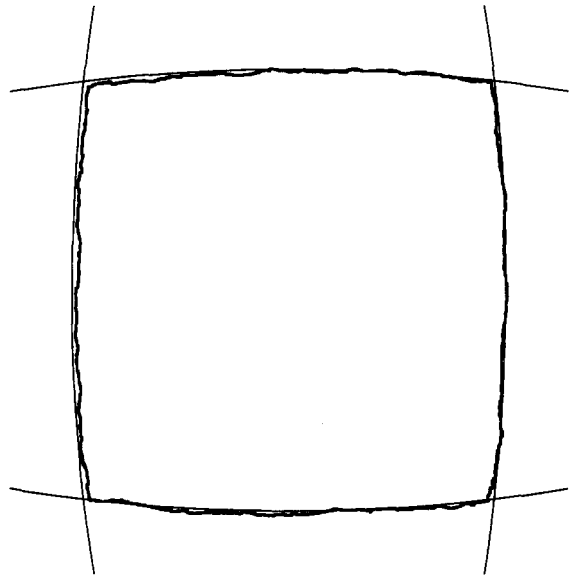

Figure 7 To characterize cluster morphologies, four equivalent elliptical arcs are fit to the boundary as explained in the text

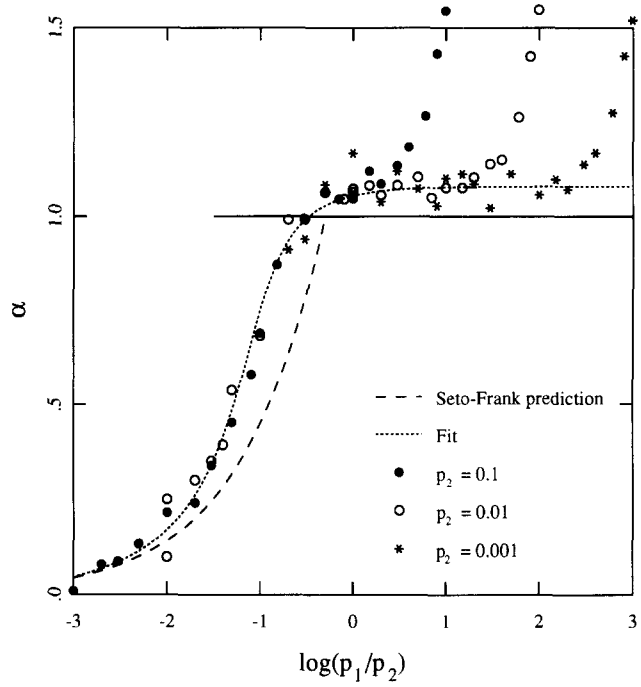

Figure 8 Variation of the shape parameter α with p_1/p_2. Symbols give simulation results; the two curves are respectively the Seto–Frank prediction, equation (10) (– – –), or the fit given by equation (11) (- - -)

except when p_1 approaches 1. The agreement with the Seto–Frank prediction is only qualitative, except when $p_1/p_2 \lesssim 10^{-2}$, i.e. when the clusters have very flat edges. The ellipses predicted by the Seto–Frank equations underestimate the actual curvature over the entire range $p_1/p_2 < \frac{1}{2}$. The actual values of α vs p_1/p_2 are represented quite well by this parametric equation:

$$\frac{p_1}{p_2} = \left(\frac{1-0.37\alpha^2}{1+2.537\alpha}\right)\frac{\alpha^2}{(2-1.47\alpha^4)} \tag{11}$$

which is also displayed in *Figure 8*. It yields two asymptotic values of α, 0 and $(1.47/2)^{1/4} = 1.08$, depending on whether p_1/p_2 is small or large. *Figure 8* displays a number of points where the best fit α is considerably

greater than 1, these correspond to values of p_1 approaching unity, are sensitive to the discrete time step and are therefore unphysical. As mentioned above, when the ratio G_r/G_0 is near 1, the simulation data are well represented by an ellipse. Computed values of G_r/G_0 are always within a few per cent of unity, implying that the best fit ellipses as given by equations (9) and (11) adequately represent the available data to within the accuracy thereof. (As one would certainly expect, G_r/G_0 is not near 1 when $p_1 \simeq 1$. The non-physical lozenges obtained in this case are not well fit by an ellipse.)

As a final comparison, we display in *Figure 9* the ratios G_0/G_{45}, first as computed by simulation with the open boundary condition, and also the predictions provided by both the Seto–Frank solution and by the fit, equation (11). (Any ellipse obeying equation (9) will yield $G_0/G_{45}=[(1+\alpha^2)/2]^{1/2}$.) This figure shows nicely the transition from the flat squares ($G_0/G_{45}=2^{-1/2}$) to the near circles ($G_0/G_{45}\simeq 1$), to the non-physical lozenges ($G_0/G_{45}=2^{1/2}$).

The regime transition is expected to occur, according to equation (8) near the point where either α or G_0/G_{45} reaches 1. Therefore we conclude that the flat, square clusters characterized by small values of p_1/p_2 are deep in regime II, and that their growth is predicted accurately by the Seto–Frank equations. The rounding that occurs as p_1/p_2 increases is predicted only qualitatively by the Seto–Frank equations, and is indicative of an impending transition to regime III. The transition to regime III occurs when the clusters have become nearly circular. The clusters continue to be nearly circular throughout regime III.

To observe a transition to regime I requires the introduction of an additional length scale, which becomes available when we consider growth with the 0° channel boundary condition. *Figure 10* displays growth rate data in that particular case. The prediction for the growth rate in regime I is:

$$G_0 = Lp_1 \qquad (12)$$

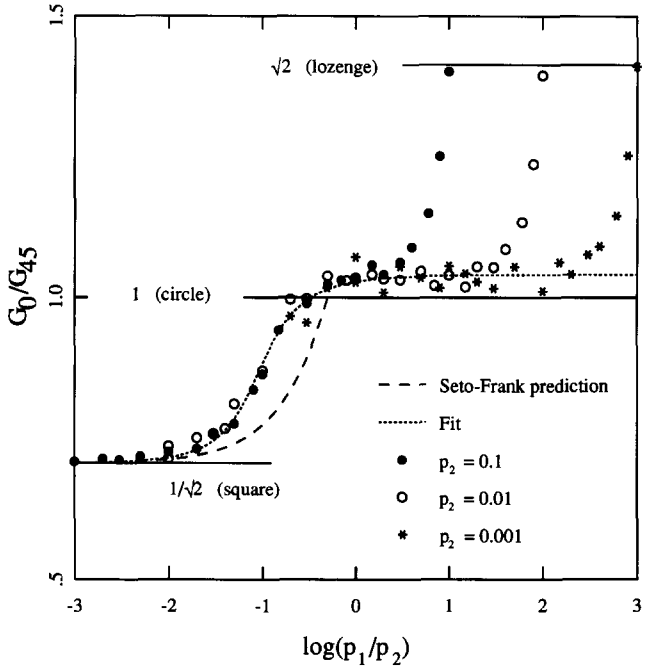

Figure 9 Variation of the ratio G_0/G_{45}. Symbols give simulation results; the two curves are respectively the Seto–Frank prediction (– – –), and the fit given by equation (11) (- - -)

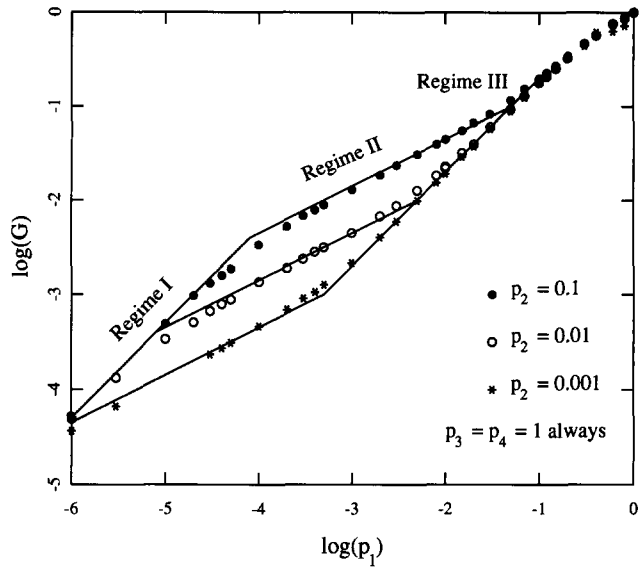

Figure 10 Growth rate data for growth in 0° channels. Symbols are simulation data, the solid lines are drawn according to equations (7), (12) and (13)

where L is the width of the channel. The crossover from regime I to regime II occurs when equations (12) and (7a) cross. Therefore, we may extend equation (8) to read:

$$\frac{p_1}{p_2} < \frac{2}{L^2} \quad \rightarrow \text{regime I} \qquad (13a)$$

$$\frac{2}{L^2} < \frac{p_1}{p_2} < 0.426 \quad \rightarrow \text{regime II} \qquad (13b)$$

$$0.426 < \frac{p_1}{p_2} \quad \rightarrow \text{regime III} \qquad (13c)$$

Figure 10 was computed using a value of $L=50$. It is obvious from *Figure 10* that the growth rates of this particular model are in good agreement with these predictions.

SUMMARY AND DISCUSSION

We have introduced a generalized Eden model as a representation for the process of polymer crystallization. The model indicates the limits of accuracy of the Seto–Frank equations. It also successfully exhibits all three growth regimes that have been well characterized both experimentally and theoretically.

The current sociological climate in the field of polymer crystallization is such that some may take exception to our claim that the data of *Figures 5* or *10* exhibit regime transitions. It will be noticed that the actual curves are much more rounded and smooth than the lines drawn according to expressions (7), (12) and (13), and that these lines severely misrepresent many of the points. (The simulation results for the 0° channel, first when $p_1=10^{-5}$ and $p_2=0.01$, and second when $p_1=0.005$ and $p_2=0.01$, are $G_0=3.36\times10^{-4}$ and $G_0=0.01274$ respectively. The predictions provided by expressions (7), (12) and (13) are respectively 33% high and 16% low.) However, the growth rate laws discussed here are excellent examples of the concept of scaling laws in physics. When one relevant parameter becomes much smaller or larger than another, the physical description often simplifies considerably and simple physical laws result. The physical

laws do not apply very well when both parameters have comparable value; the physical description is usually much more complicated in such 'crossover' regions. (If we had unlimited computer resources, we could study the model over a much broader range of input parameters and observe well delineated regimes. For example, the condition for regime II is $b \ll L_f \ll L$. When we set $L = 50b$, we do not provide an extremely broad range for regime II to develop.) Therefore, it may be more proper to refer to regime crossovers than to regime transitions, but the nomenclature seems already to be well set. Also it is usually the case that quantities such as i and g are strong functions of temperature, changing by many orders of magnitude as the temperature changes only a few degrees. With this model we do not see abrupt regime transitions since we work directly with the parameters p_1, p_2, etc. In nature the transitions can be much more abrupt if viewed, for example, as functions of temperature.

The growth-front curvature observed either with this model or as approximated by the elliptical-profile solutions to the Seto–Frank equations is now seen to be a direct consequence of the proximity of regime III. Specifically, there is no need to modify or replace the traditional kinetic nucleation model of polymer crystallization[3–5] with the surface roughening notions proposed by Sadler[13–21]. Curved growth fronts appear to be the expected morphology of polymer single crystals grown in or near regime III. This has probably gone unnoticed because of the difficulty of obtaining single crystals in regime III. In fact, the standard Eden cluster appears to be the predicted structure of regime III single crystals. We note that DiCorleto and Bassett have reported single crystals of polyethylene having circular morphology[10]. The regime in which these crystals were grown is not known, but regime III growth is not an unreasonable assumption.

Regimes I and II correspond to the more traditional view of polymer nucleation theory, in which a single nucleation event (i.e. the p_1-process in our model) gives rise, through substrate completion (i.e. the p_2-process), to the crystallization of a large number of polymer stems. Regime III, and the resultant curved edges, is a more recent extension of the same ideas to the situation when substrate completion becomes less important. Apparently, there are those who object to using the phrase 'nucleation' to refer to this more recent extension, but it is important to note that the issue is really only one of semantics.

Despite the success of this model in predicting regimes I, II and III, and in predicting growth front curvature, there are certain ways in which the model is too simple. Particularly, the standard Eden model and its generalization studied here can contain voids, especially under conditions corresponding to regime III. In order to eliminate voids, it would be necessary to modify the model along the lines already considered by other authors[54,56–58]. In these studies, constraints are applied specifically to eliminate voids. We are confident that such constraints will appreciably affect neither the global cluster structure nor the overall growth rates, although they certainly affect the fine structure of the boundary.

ACKNOWLEDGEMENTS

The authors are grateful to Drs John D. Hoffman and Robert L. Miller for their encouragement of this research. Partial financial support was provided by the National Science Foundation, grant DMR-8822934.

REFERENCES

1 Seto, T. *Rep. Prog. Polym. Phys. Japan* 1964, **7**, 67
2 Frank, F. C. *J. Cryst. Growth* 1974, **22**, 233
3 Hoffman, J. D. and Lauritzen, J. I. *J. Res. Natl Bur. Stand. USA* 1961, **65A**, 297
4 Hoffman, J. D. *Soc. Plastics Eng. Trans.* 1964, **4**, 315
5 Hoffman, J. D., Davis, G. T. and Lauritzen, J. I. in 'Treatise on Solid State Chemistry' (Ed. N. B. Hannay), Vol. 3, Plenum Press, New York, 1976
6 Organ, S. J. and Keller, A. *J. Mater. Sci.* 1985, **20**, 1571
7 Organ, S. J. and Keller, A. *J. Mater. Sci.* 1985, **20**, 1586
8 Organ, S. J. and Keller, A. *J. Mater. Sci.* 1985, **20**, 1602
9 Organ, S. J. and Keller, A. *J. Polym. Sci., Polym. Phys. Edn* 1986, **24B**, 2319
10 DiCorleto, J. A. and Bassett, D. C. *Polymer* 1990, **31**, 1971
11 Toda, A. *Polymer* 1991, **32**, 771
12 Toda, A. *Colloid. Polym. Sci.* 1992, **270**, 667
13 Sadler, D. M. and Gilmer, G. H. *Polymer* 1984, **25**, 1446
14 Sadler, D. M. *J. Polym. Sci., Polym. Phys. Edn* 1985, **23**, 1533
15 Sadler, D. M. *Polym. Commun.* 1986, **27**, 140
16 Sadler, D. M. and Gilmer, G. H. *Phys. Rev. Lett.* 1986, **56**, 2708
17 Sadler, D. M. *J. Chem. Phys.* 1987, **87**, 1771
18 Sadler, D. M. *Polymer* 1987, **28**, 1440
19 Goldbeck-Wood, G. and Sadler, D. M. *Polym. Commun.* 1990, **31**, 143
20 Goldbeck-Wood, G. *Polymer* 1990, **31**, 586
21 Armistead, K. and Goldbeck-Wood, G. *Adv. Polym. Sci.* 1992, **100**, 219
22 Mansfield, M. L. *Polymer* 1988, **29**, 1755
23 Mansfield, M. L. *Polym. Commun.* 1990, **31**, 283
24 Toda, A. *Faraday Disc. Chem. Soc.* 1993, **95**, 129
25 Mansfield, M. L. *Polymer*, 1993, **34**, 4904
26 Hoffman, J. D. and Miller, R. L. *Macromolecules* 1989, **22**, 3038
27 Miller, R. L. and Hoffman, J. D. *Polymer* 1991, **32**, 963
28 Peters, H. P., Stauffer, D., Holters, H. P. and Loewenich, K. *Z. Physik B* 1979, **34**, 399
29 Vannimenus, J., Nickel, B. and Hakim, V. *Phys. Rev. B* 1984, **30**, 391
30 Plischke, M. and Racz, Z. *Phys. Rev. Lett.* 1984, **53**, 415
31 Parisi, G. and Zhang, Y.-C. *Phys. Rev. Lett.* 1984, **53**, 1791
32 Dhar, D. *Phys. Rev. Lett.* 1985, **54**, 2058
33 Freche, P., Stauffer, D. and Stanley, H. E. *J. Phys. A: Math. Gen.* 1985, **18**, L1163
34 Meakin, P., Jullien, R. and Botet, R. *Europhys. Lett.* 1986, **1**, 609
35 Witten, T. A. and Cates, M. E. *Science* 1986, **232**, 1607
36 Zabolitzky, J. G. and Stauffer, D. *Phys. Rev. A* 1986, **34**, 1523
37 Stauffer, D. *J. Phys. A: Math. Gen.* 1986, **19**, 3933
38 Hirsch, R. and Wolf, D. E. *J. Phys. A: Math. Gen.* 1986, **19**, L251
39 Zheng, W. M. *Phys. Rev. A* 1987, **35**, 4904
40 Wolf, D. E. and Kertesz, J. *J. Phys. A: Math. Gen.* 1987, **20**, L257
41 Meakin, P. *J. Phys. A: Math. Gen.* 1987, **20**, L1113
42 Meakin, P. *Phys. Rev. A* 1988, **38**, 418
43 Kertesz, J. and Wolf, D. E. *J. Phys. A: Math. Gen.* 1988, **21**, 747
44 Amitrano, C., Coniglio, A. and diLiberto, F. *J. Phys. A: Math. Gen.* 1988, **21**, L201
45 Devillard, P. and Stanley, H. E. *Phys. Rev. A* 1988, **38**, 6451
46 Jiang, Y., Gang, H. and Ben-Kun, M. *Phys. Rev. B* 1989, **39**, 4572
47 Devillard, P. and Stanley, H. E. *Physica A* 1989, **160**, 298
48 Vicsek, T., Cserzo, M. and Horvath, V. K. *Physica A* 1990, **167**, 315
49 deArcangelis, L. and Herrmann, H. J. *J. Phys. A: Math. Gen.* 1990, **23**, L923
50 Batchelor, M. T. and Henry, B. I. *Phys. Lett. A* 1991, **157**, 229
51 Poland, D. *J. Phys. A: Math. Gen.* 1991, **24**, 229
52 Roux, S., Hansen, A. and Hinrichsen, E. L. *J. Phys. A: Math. Gen.* 1991, **24**, L295
53 Bennett, C. H., Buttiker, M., Landauer, R. and Thomas, H. *J. Stat. Phys.* 1981, **24**, 419
54 Guttman, C. M. and DiMarzio, E. A. *J. Appl. Phys.* 1983, **54**, 5541
55 Goldenfeld, N. *Polym. Commun.* 1984, **25**, 47
56 Toda, A. and Tanzawa, Y. *J. Cryst. Growth* 1986, **76**, 462
57 Gates, D. J. and Westcott, M. *Proc. R. Soc. Lond.* 1988, **A416**, 443
58 Gates, D. J. and Westcott, M. *Proc. R. Soc. Lond.* 1988, **A416**, 463
59 Ball, R. C. and Brady, R. M. *J. Phys. A: Math. Gen.* 1985, **18**, L809